AIP | Physics of Fluids

Apparent dynamic contact angle of an advancing gas–liquid meniscus

Serafim Kalliadasis and HsuehChia Chang

Citation: Physics of Fluids (1994-present) **6**, 12 (1994); doi: 10.1063/1.868076
View online: http://dx.doi.org/10.1063/1.868076
View Table of Contents: http://scitation.aip.org/content/aip/journal/pof2/6/1?ver=pdfcov
Published by the AIP Publishing

Articles you may be interested in

Measurement of dynamic/advancing/receding contact angle by videoenhanced sessile drop tensiometry
Rev. Sci. Instrum. **67**, 2852 (1996); 10.1063/1.1147117

Direct numerical simulation of nearinterface turbulence in coupled gasliquid flow
Phys. Fluids **8**, 1643 (1996); 10.1063/1.868937

The breakdown of asymptotic hydrodynamic models of liquid spreading at increasing capillary number
Phys. Fluids **7**, 2631 (1995); 10.1063/1.868711

The caloric effect of adsorption at the electrified metal/electrolyte interface
J. Chem. Phys. **103**, 6164 (1995); 10.1063/1.470443

The role of surface tension in the dominant balance in the die swell singularity
Phys. Fluids **7**, 2328 (1995); 10.1063/1.868746

This article is copyrighted as indicated in the article. Reuse of AIP content is subject to the terms at: http://scitation.aip.org/termsconditions. Downloaded to IP: 128.118.88.48 On: Fri, 05 Dec 2014 10:14:59

Apparent dynamic contact angle of an advancing gas–liquid meniscus

Serafim Kalliadasis and Hsueh-Chia Chang
Department of Chemical Engineering, University of Notre Dame, Notre Dame, Indiana 46556

(Received 23 March 1993; accepted 24 August 1993)

The steady motion of an advancing meniscus in a gas-filled capillary tube involves a delicate balance of capillary, viscous, and intermolecular forces. The limit of small capillary numbers Ca (dimensionless speeds) is analyzed here with a matched asymptotic analysis that links the outer capillary region to the precursor film in front of the meniscus through a lubricating film. The meniscus shape in the outer region is constructed and the apparent dynamic contact angle Θ that the meniscus forms with the solid surface is derived as a function of the capillary number, the capillary radius, and the Hamaker's constant for intermolecular forces, under conditions of weak gas–solid interaction, which lead to fast spreading of the precursor film and weak intermolecular forces relative to viscous forces within the lubricating film. The dependence on intermolecular forces is very weak and the contact angle expression has a tight upper bound $\tan\Theta = 7.48\ \mathrm{Ca}^{1/3}$ for thick films, which is independent of the Hamaker constant. This upper bound is in very good agreement with existing experimental data for wetting fluids in any capillary and for partially wetting fluids in a prewetted capillary. Significant correction to the $\mathrm{Ca}^{1/3}$ dependence occurs only at very low Ca, where the intermolecular forces become more important and $\tan\Theta$ diverges slightly from the above asymptotic behavior toward lower values.

I. INTRODUCTION

The motion of an apparent contact line formed at the intersection of two immiscible fluids with a solid substrate is a complex process that appears in many practical applications.[1] One theoretical approach to this problem is to allow slip at the contact line. However, this introduces a nonintegrable stress singularity at the contact line.[2,3] Hocking[4] showed that the moving contact line model can be analyzed with the method of matched asymptotic expansions: an inner region, very close to the contact line, where a slip boundary condition is applied, has to be matched with an outer region away from the contact line, where the full Navier–Stokes equation applies. Ngan and Dussan[5] have shown that the dynamics of the fluids in the outer region depends essentially on only one parameter, which, in turn, depends on the actual dynamic contact angle in the inner region (the angle that the fluid–fluid interface forms with the solid wall) and the slip length scale. It is impossible to *a priori* deduce unique values for the contact angle or the slip length scale. Slip models[6] have to be introduced, and the entire flow field has to be resolved in this approach before the dependence of the apparent dynamic contact angle in the outer region as a function of the pertinent parameters, such as the capillary number, can be determined.

However, experimental studies conducted on moving contact lines between a liquid and a gas by Hoffman,[7] Tanner,[8] Rose and Heinz,[9] and many others show that with liquids that wet the solid under static conditions, the apparent dynamic contact angle Θ that the liquid forms with the solid surface is closely described by a universal relationship at low speeds, known sometimes as Tanner's law,

$$\Theta \sim \text{const}\ \mathrm{Ca}^{1/3}, \tag{1}$$

where $\mathrm{Ca} = \mu U/\sigma$ is the capillary number, μ and σ are the viscosity and the interfacial tension of the liquid phase, and U is the velocity of the contact line. The constant seems to be independent of the solid–liquid–gas combination, as long as the liquid wets the solid at zero Ca or if the capillary is prewetted. This suggests that the apparent contact angle involves a balance of capillary and viscous forces with intermolecular forces playing only a secondary role. As such, one suspects for wetting fluids the existence of a thin lubricating film in front of the meniscus that is invisible to the naked eye. The contact line is hence just an outer region illusion. This film has now been experimentally verified and is an integral part of modern modeling approaches to the apparent contact angle problem. It also suggests that the apparent dynamic contact angle of wetting fluids at low Ca can be derived from basic principles involving simple forces—slip models are unnecessary for these fluids. Part of the physical picture is clear. By balancing capillary forces to viscous forces for a thin film, one obtains the typical lubrication scalings of $\mathrm{Ca}^{2/3}$ and $\mathrm{Ca}^{1/3}$ for the vertical and horizontal length scales of the liquid film region in front of the meniscus[10] (see Fig. 1). These scalings yield the Ca dependence of the empirical correlation in (1). A similar derivation using energy dissipation arguments by Hervert and De Gennes[11] also leads to the same scaling $\Theta \sim \mathrm{Ca}^{1/3}$. However, to determine the constant, one must resolve the asymptotic behavior of the film in both the front and the back with a matched asymptotic

 1070-6631/94/6(1)/12/12/$6.00 © 1994 American Institute of Physics

This article is copyrighted as indicated in the article. Reuse of AIP content is subject to the terms at: http://scitation.aip.org/termsconditions. Downloaded to IP: 128.118.88.48 On: Fri, 05 Dec 2014 10:14:59

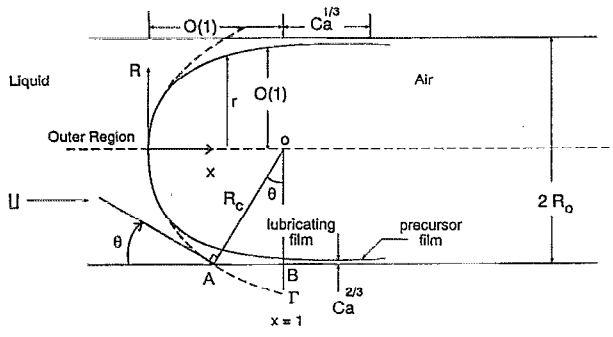

FIG. 1. Schematic of the meniscus with proper scalings of the outer static and lubrication film regions. The measured contact angle is an extrapolation of the outer static region toward the capillary wall.

analysis. In front of the lubricating film, one expects the interface to approach molecular scales as intermolecular forces become important. The presence of this molecular precursor film has now been verified both experimentally[12] and from molecular dynamics simulations.[13] Behind the lubricating film, the length scales become very large. For an advancing meniscus in a capillary, as shown in Fig. 1, both horizontal and vertical length scales are of the order of the capillary radius R_0 in this outer region. For the case of a spreading drop on a flat surface, the initial outer region when gravity is important has length scales corresponding to the capillary length scale $(\sigma/\rho g)^{1/2}$. Determination of the constant for Tanner's law then involves matching of solutions to these regions of widely different length scales.

The first attempt to derive the constant was by Voinov[14] for the spreading of drops on a plane. Perhaps because Tanner[8] measured the contact angle Θ at a point in the outer region where the curvature of the interface vanishes, Voinov found an inner solution whose slope varies as one-third power of the logarithm of the film thickness. As a result, the second derivative vanishes when the interfacial height blows up to infinity as it enters the outer region in the back. An expression of the form

$$\Theta^3 \sim \Theta_m^3 + 9\ \mathrm{Ca}\ \ln(H/H_m)$$

was obtained, where Θ is the local slope of the interface with height H while Θ_m and H_m are the infinitesimally small slope and height at an arbitrary position at the front near the precursor film. Since there is no matching with the front-running precursor film where the continuum model breaks down, Θ_m and H_m are unknown. Moreover, the slope Θ does not approach an asymptotic value as $H \to \infty$ into the outer region. As a result, although the superficial scaling of Tanner's law is reproduced, the constant remains essentially unknown. A recent derivation of the same expression is offered by De Gennes,[15] although H_m and Θ_m are sometimes replaced by analogous and equally unknown characteristic horizontal scales. Friz[16] attempted the matched asymptotic analysis for the advancing meniscus problem of Fig. 1 by assuming a macroscopic constant-thickness precursor film in front with an unspecified thickness. He located an inner solution that blows up linearly as it approaches the outer region at the back. With this stipulation, it can be shown that the constant asymptotic slope of the inner solution at the back is essentially independent of the unknown film thickness. He derived a constant of 3.4 with this approach, which is significantly lower than the experimental data. (Our final value is 7.48). From the capillary experiments, however, it is evident that the film evolves into a static sphere in the outer region of the meniscus. In fact, the contact angle is obtained experimentally by extrapolating the outer region towards the capillary wall,[7] as shown in Fig. 1. We shall show that a linear asymptotic behavior for the film solution can never allow proper matching with the static outer region and hence the apparent contact angle would not be properly resolved. The dynamic contact angle corresponds to an extrapolation of the outer solution toward the capillary wall and *not* an extrapolation of the inner solution toward the outer region at the back.

In this paper, we carry out a complete matched asymptotic analysis of the advancing meniscus problem in Fig. 1. The nonstationary drop spreading problem is more difficult and will be addressed in a follow-up paper. The physical model and the analysis are quite similar, however, for both apparent contact angle problems. We examine the interesting limit of a fast wetting fluid with a large spreading coefficient S, defined as the net force at the tip of the precursor film $S=\sigma_{SG}-\sigma_{SL}-\sigma$, where the various σ correspond to solid–gas, solid–liquid, and gas–liquid interfacial tension, respectively. This implies that the tip of the precursor film is essentially at infinity from the meniscus and it is hence decoupled from the problem, even when the meniscus is advancing. We can then formulate a stationary problem for the advancing meniscus in a moving frame without explicit consideration for the spreading of the precursor film. The lubricating film simply approaches zero thickness smoothly at an infinite distance from the meniscus. (Our theory is also appropriate for partially wetting fluids if the capillary is prewetted. In this case, rapid spreading of the liquid is not required.) We shall be mostly interested in the limit where the viscous force is in excess of the intermolecular forces within the film, even as the precursor film is approached. This will be shown to be true for most wetting liquids at Ca beyond 10^{-5}. One expects a fast-wetting fluid with a high spreading coefficient S to have weak attractive intermolecular forces between the gas and solid molecules on either side of the liquid film. This is because the advancement of the precursor film in the wetting process involves the separation of the gas molecules from the solid ones. These two limits are hence quite compatible. In these fast-spreading and small-intermolecular-force limits, we derive the constant for Tanner's law as a function of the Hamaker's constant, the capillary radius, and the surface tension of the fluid. A tight upper bound of 7.48 for the coefficient in front of Tanner's law, which is independent of S or the Hamaker's constant, is also derived for thick films. Based on this value, the predicted dynamic contact angle is shown to be in good agreement with experimental data. The matched asymptotic analysis includes proper matching between the outer region and the lubrication region and a proper approach toward the precursor film. The

This article is copyrighted as indicated in the article. Reuse of AIP content is subject to the terms at: http://scitation.aip.org/termsconditions. Downloaded to IP: 128.118.88.48 On: Fri, 05 Dec 2014 10:14:59

weak dependence of the contact angle on the intermolecular forces destroys the $Ca^{1/3}$ dependence of Θ at very low Ca, where the thin film allows intermolecular forces to reduce Θ.

II. FORMULATION

A liquid slug displaces air slowly in a capillary tube of diameter $2R_0$ (Fig. 1). The slug moves with constant speed U with respect to a laboratory frame of reference, and when U is low, the air–liquid interface bows out into the liquid phase. For relatively small R_0 with a small Bond number, gravitational effects can be neglected, and a coordinate system (x,R) that moves with the interface is used. Equivalently, the wall moves with velocity $-U$ with respect to the system (x,R). The Stokes approximation will be used, and, for simplicity, the viscosity of the gas phase is assumed to be zero, so that the dynamics of the two fluids is essentially decoupled. The gas pressure is then a constant $(=P_g)$, and only the dynamics of the liquid phase will be considered. The equations of change and the appropriate boundary conditions are nondimensionalized with the scales $\{\mathbf{x},\mathbf{u},P\}\sim\{R_0,U,\sigma/R_0\}$, where σ is the surface tension of the liquid.

We will initially divide the domain of interest into two regions: the outer region where the lateral and vertical length scales are both $O(1)$ as pressure and surface tension forces balance, and the inner lubrication region in which the lateral and vertical length scales are $O(Ca^{1/3})$ and $O(Ca^{2/3})$, respectively, as capillary and viscous forces balance.[10,17] Further division of the inner region will be necessary when the intermolecular forces become important at very thin films. In the outer region, viscous effects enter at $O(Ca)$. The equation that describes the meniscus shape, valid up to $O(Ca^{2/3})$, is then the axisymmetric Laplace–Young equation that describes the static normal stress balance on the free surface $r(x)$,

$$P-P_g=\frac{r_{xx}}{(1+r_x^2)^{3/2}}-\frac{1}{r(1+r_x^2)^{1/2}}, \quad \text{at } R=r, \tag{2}$$

where the interface is defined as $R=r$, with r being the radial position corresponding to distance x from the tip of the meniscus. The following tip boundary conditions will be used for the static meniscus:

$$r(0)=0, \tag{3a}$$

$$r_x(x\to 0^+)\to+\infty\,. \tag{3b}$$

The region $r\to 1$ is the inner domain, which is planar to all pertinent leading orders in Ca. The balance between surface tension and viscous forces in the inner region can be made more precise by introducing the inner variables,

$$X=(x-\zeta)Ca^{-1/3}, \quad Y=(-R+1)Ca^{-2/3}, \quad H=(-r+1)Ca^{-2/3}, \tag{4}$$

where $x=\zeta(>0)$ represents the location of the origin for the coordinate system (X,H). We will include long-range attractive van der Waals intermolecular interactions, which can be added to the momentum equations of motion as extra distributed body forces.[18] In the lubrication limit, this corresponds to an extra term in the liquid pressure,

$$P=P_g-\sigma z_{xx}+\frac{A}{6\pi z^3}, \tag{5}$$

where z is the film thickness. This then leads to the evolution equation,

$$z_t+\frac{1}{3\mu}\frac{\partial}{\partial x}\left[z^3\frac{\partial}{\partial x}\left(\sigma z_{xx}-\frac{A}{6\pi z^3}\right)\right]=0, \tag{6}$$

for the inner region, where $(\,)_t$ denotes differentiation with respect to time. The term $A/6\pi z^3$ in (6) is known as the "disjoining pressure" and the parameter A is the Hamaker's constant. It is negative for wetting fluids.[14] For nonpolar or slightly polar materials, London and van der Waals forces are the main source of attraction between the molecules. These forces can be represented with a potential function $\Phi=A/6\pi z^3$. This expression can be derived by using an r_{ij}^{-7} potential for the energy of interaction between two molecules, i and j, of two different species. This potential is appropriate for relatively large separation distances (of the order of tens of nanometers) so that "retardation effects" must be considered. The above expression for Φ is then derived by integrating the interaction potential in space. The final result represents the interaction between two different phases separated by a third phase[19] of uniform thickness z. The same form for the intermolecular potential can be used for a nearly uniform film thickness z, provided that $|z_x|\ll 1$. This nearly parallel approximation has also been invoked for the lubrication approximation. We shall demonstrate that all our solutions obey this approximation. As a result, we are restricted to menisci with small contact angles. For large contact angles where the slope of the film interface is not necessarily small, (6) must be corrected for nonparallel effects.[20] These correction terms are negligibly small for the small contact angle menisci that are of interest here.

One needs to be careful in introducing intermolecular forces into a continuum model like the Navier–Stokes equation. In particular, the surface tension force, which is due to intermolecular forces between the gas and liquid phases, cannot be considered separately from the van der Waals forces between the gas and solid phases for very thin films. If one introduces the molecular length scale R_m,

$$R_m=(|A|/6\pi\sigma)^{1/2}, \tag{7a}$$

or its dimensionless counterpart,

$$\lambda=R_m/R_0; \tag{7b}$$

the above model for the lubricating film is valid if its film thickness is much larger than R_m, viz., $Ca^{2/3}\gg\lambda$. Since R_m is typically of the order of a few Ångströms, while a typical capillary radius is 1 mm, the lower bound on Ca is $\sim 10^{-5}$. Beyond this lower bound, the continuum model remains valid for the lubricating film. We also expect intermolecular forces to be less effective at relatively large $Ca\gg 10^{-5}$, such that the dependence of Tanner's law on λ becomes progressively more weak. Nevertheless, this limitation prevents us from resolving the film to the Ångström level as it

This article is copyrighted as indicated in the article. Reuse of AIP content is subject to the terms at: http://scitation.aip.org/termsconditions. Downloaded to IP: 128.118.88.48 On: Fri, 05 Dec 2014 10:14:59

approaches the precursor film in front that exists at any value of Ca. Fortunately, this resolution is not required, since we only need to know the asymptotic behavior of the lubricating film in regions where the continuum assumption still holds, and the disjoining pressure can be safely included in the formulation. It is also fortunate that we do not need to resolve the motion of the precursor film. Here, nonstationary molecular interaction surely dominates, and it is difficult to reconcile it with our stationary formulation. In essence, we are concerned with a fast wetting liquid with a large spreading coefficient. The experimental investigations by Ausserré *et al.*[12] for spreading of small droplets of high molecular weight polymer liquids on solid surfaces show that, for about 1 h after the beginning of the spreading, the speed of spreading corresponds to a capillary number of 0.01. One then expects that for liquids of much smaller viscosity, the precursor film moves even faster, with a speed far larger than the meniscus speed U at low Ca. The fast moving tip of the precursor film then essentially runs itself out of the picture. At larger Ca, the meniscus speed will exceed the wetting speed and the meniscus will reverse its curvature as the contact angle Θ passes through 90°. Hence our analysis is only valid for small Θ. The front of the precursor film also disappears if the capillary is prewetted. We will show that our theory also applies to this case, even when the fluid is partially wetting on a dry surface under static conditions.

Introducing the moving coordinate transformation for our stationary formulation,

$$x \to x - Ut, \tag{8}$$

and with $A = -|A|$, Eq. (6) is written as

$$-Uz_x + \frac{1}{3\mu}\left[z^3\left(\sigma z_{xx} + \frac{|A|}{6\pi z^3}\right)_x\right]_x = 0. \tag{9}$$

With $z \to z/R_0$ and $x \to x/R_0$, (9) becomes

$$-\mathrm{Ca}\, z_x + \frac{1}{3}\left[z^3\left(z_{xx} + \frac{\lambda^2}{z^3}\right)_x\right]_x = 0. \tag{10}$$

Integrating (10) once and setting the integration constant equal to zero, we derive the basic equation for the inner region,

$$z^3 z_{xxx} = 3\,\mathrm{Ca}\, z + \frac{\lambda^2}{z} z_x. \tag{11}$$

With $x = \zeta + X\,\mathrm{Ca}^{1/3}$, $z = H\,\mathrm{Ca}^{2/3}$ (11) yields

$$H^3 H_{XXX} = 3H + \frac{\lambda^2}{\mathrm{Ca}^2}\frac{H_X}{H}. \tag{12}$$

The solution of the above equation has to be matched to the outer solution r. The matching condition can be written as

$$-r(x \to \zeta) + 1 \sim \mathrm{Ca}^{2/3} H(X \to -\infty). \tag{13}$$

Such matched asymptotic analysis of related problems is first introduced by Park and Homsy[17] in the study of a two-phase flow in a Hele–Shaw cell. Their analysis clarified Bretherton's work[10] for the motion of a long gas bubble in a capillary. However, in all these studies of bubbles, a finite film thickness exists in front of the back meniscus. The inner solution departing from the flat film region is then matched to the outer solution. In the present study, our meniscus is analogous to the back meniscus of a bubble, but the thickness of the inner region approaches zero as the precursor film is approached. Since the fluid spreads rapidly, the precursor film thickness is vanishingly small compared to the lubricating film and the integration constant in (11) is set equal to zero. This shape of the lubricating film is consistent with the experimental measurement of Ausserré *et al.*[12] The condition

$$H(X \to +\infty) \to 0^+ \tag{14}$$

is hence imposed in the front of the meniscus. In fact, we shall show that H decays hyperbolically toward zero in Sec. IV due to vanishingly small intermolecular forces between the gas and solid molecules across the liquid film. However, since the continuum model breaks down when the dimensionless film thickness $1-r$ is of order λ, the zero film thickness limit actually corresponds to $H\,\mathrm{Ca}^{2/3}$ approaching $O(\lambda)$.

III. MATCHING

Substituting into the outer equation (2) the expansions

$$r \sim r_0 + \mathrm{Ca}^{1/3} r_1 + \mathrm{Ca}^{2/3} r_2, \tag{15a}$$

$$P \sim P_0 + \mathrm{Ca}^{1/3} P_1 + \mathrm{Ca}^{2/3} P_2, \tag{15b}$$

one obtains a system of equations for r_0, r_1, and r_2 subject to the boundary conditions (3a) and (3b). The r_0 equation is simply

$$-\Delta P_0 = P_0 - P_g = \frac{r_0''}{[1+(r_0')^2]^{3/2}} - \frac{1}{r_0[1+(r_0')^2]^{1/2}}, \tag{16}$$

where ΔP_0 is expected to be a positive quantity. The prime denotes differentiation with respect to x. The solution to (16) can be obtained by introducing the transformation

$$r_0 = F(y), \quad y = [1+(r_0')^2]^{1/2}, \tag{17a}$$

such that (16) becomes

$$\frac{dy}{dF} = \frac{1}{F}y - (\Delta P_0)y^2, \tag{17b}$$

which can be further transformed with

$$y = W^{-1}, \tag{17c}$$

to a linear differential equation,

$$\frac{dW}{dF} = (\Delta P_0) - \frac{1}{F}W. \tag{17d}$$

Once the function $y(F) = y(r_0) = [1+(r_0')^2]^{1/2}$ is known, r_0 can be easily determined from boundary conditions (3). The solution involves inversion of an elliptic integral, and is simply

$$r_0 = \frac{2}{\Delta P_0}\left[1 - \left(1 - \frac{\Delta P_0}{2}x\right)^2\right]^{1/2}. \tag{18}$$

This article is copyrighted as indicated in the article. Reuse of AIP content is subject to the terms at: http://scitation.aip.org/termsconditions. Downloaded to IP: 128.118.88.48 On: Fri, 05 Dec 2014 10:14:59

The following matching conditions are obtained from (13) up to $O(\mathrm{Ca}^{1/3})$:

$$O(\mathrm{Ca}^0 X^0): \quad r_0(\zeta)=1, \tag{19a}$$

$$O(\mathrm{Ca}^{1/3} X^0): \quad r_1(\zeta)=0, \tag{19b}$$

$$O(\mathrm{Ca}^{1/3} X^1): \quad r_0'(\zeta)=0, \tag{19c}$$

where the prime denotes differentiation with respect to x. Equation (18), with the help of (19a) and (19c), yields

$$\Delta P_0=2, \tag{20a}$$

$$\zeta=1. \tag{20b}$$

This specifies the leading-order curvature corresponding to a half-sphere with radius R_0 and the matching location $\zeta=1$. A half-sphere with radius R_0 yields a zero apparent contact angle. It corresponds to the static meniscus at zero Ca for a wetting fluid, or, more precisely, the vanishingly small apparent dynamic contact angle at small Ca. (Hence we include partially wetting fluids that do not have zero static contact angles but have vanishingly small dynamic contact angles in a prewetted capillary.)

The next-order equation in (2) for the shape correction r_1 yields the solution

$$r_1=\frac{P_1}{2}\frac{x}{[1-(1-x)^2]^{1/2}}. \tag{21}$$

Application of the matching condition (19b) leads to

$$r_1=\frac{P_1}{2}=0, \tag{22}$$

and the first nontrivial correction to the meniscus shape is at $O(\mathrm{Ca}^{2/3})$.

Matching of the next-order terms requires an asymptotic inner solution to match $r_0''(1)$, the nonzero curvature of the static sphere at $\zeta=1$. This then stipulates that the inner solution must behave quadratically in the asymptotic limit of $X\to-\infty$. It immediately rules out the possibility of a linear asymptotic behavior for the inner solution.[16] In the limit of $X\to-\infty$, H becomes infinitely large and the solution of (12) behaves quadratically, in general,

$$H\sim\tfrac{1}{2}C\tilde{X}^2+b\tilde{X}+a, \quad \text{as } \tilde{X}\to-\infty \tag{23a}$$

or

$$H\sim\tfrac{1}{2}CX^2+\tilde{b}X+\tilde{a}, \quad \text{as } X\to-\infty, \tag{23b}$$

where

$$\tilde{X}=X+\tau, \tag{24a}$$

$$\tilde{b}=b+C\tau, \tag{24b}$$

$$\tilde{a}=a+b\tau+\tfrac{1}{2}C\tau^2, \tag{24c}$$

and τ represents an arbitrary shift of the coordinate X, since (12) is invariant under translation. The proper shift will be selected by matching. An inner region that behaves linearly as $X\to-\infty$ has been invoked by Friz,[16] where (12), without molecular forces and with the presence of the term -3 at the right-hand side corresponding to a constant film thickness as $X\to+\infty$, is integrated numerically, so that a linear behavior is obtained. Indeed, one can find appropriate "initial" conditions for (12), such that the inner solution (introduced first by Bretherton[10]) behaves linearly away from the wall. However, no matching with the outer region is possible in this case. The following matching conditions can now be obtained to $O(\mathrm{Ca}^{2/3})$:

$$O(\mathrm{Ca}^{2/3} X^2): \quad -\frac{1}{2!}r_0''(1)=\frac{1}{2}C, \tag{25a}$$

$$O(\mathrm{Ca}^{2/3} X^1): \quad -r_1'(1)=\tilde{b}, \tag{25b}$$

$$O(\mathrm{Ca}^{2/3} X^0): \quad -r_2(1)=\tilde{a}. \tag{25c}$$

From (25a) and (25b) we obtain

$$C=1, \tag{26a}$$

$$\tilde{b}=0, \tag{26b}$$

and the shift τ can be determined from (26b) as

$$\tau=-b/C, \tag{26c}$$

while (24c) gives

$$\tilde{a}=a-\frac{b^2}{2C}, \tag{26d}$$

and H in (23b) can be simply written as

$$H\sim\tfrac{1}{2}X^2+\tilde{a}, \quad \text{as } X\to-\infty. \tag{27}$$

We shall demonstrate that $\tilde{a}$ is a negative parameter. The asymptotic parabolic behavior of H away from the capillary wall, as represented by (27), can then be extrapolated back toward the capillary wall, and its minimum at $X=0$ actually lies below the capillary wall. We shall show that the apparent contact angle, instead of being the slope of H at large H, which obviously does not converge, is the slope of H at $H=0$!

We are now ready to resolve the first nontrivial correction to the static meniscus that also yields the correction to the zero contact angle at vanishing Ca. The $\mathrm{Ca}^{2/3}$ equation for r_2 in (2) yields

$$r_2=\frac{P_2}{2}\frac{x}{[1-(1-x)^2]^{1/2}}, \tag{28}$$

and, after applying the matching condition (25c),

$$\frac{P_2}{2}=-\tilde{a}, \tag{29}$$

which completes the matching between r and H. The constant $\tilde{a}$ represents the curvature correction and hence the apparent dynamic contact angle due to capillary-driven flow into the inner region. Its value is determined from the asymptotic behavior of the inner solution, which will be constructed in the next section.

IV. THE INNER REGION

The inner region represented by Eq. (12) can be further divided into three subregions (Fig. 2): the original lubrication region (a), where the capillary term H^3H_{xxx} and the viscous term $3H$ balance, a transition region (b),

This article is copyrighted as indicated in the article. Reuse of AIP content is subject to the terms at: http://scitation.aip.org/termsconditions. Downloaded to IP: 128.118.88.48 On: Fri, 05 Dec 2014 10:14:59

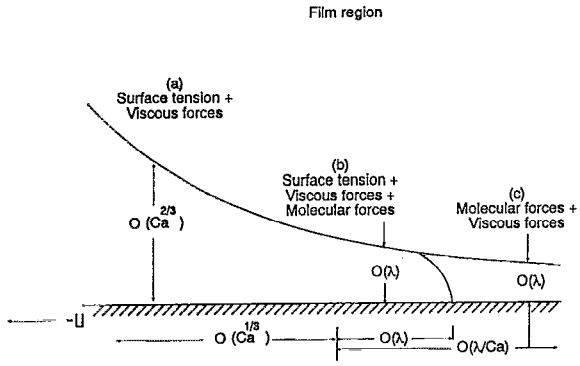

FIG. 2. Scaling and dominant forces of the segment connecting the lubrication film and precursor film regions. A tip singularity with length scales λ can appear at a finite distance from the meniscus for some inner solutions. The correct inner solution decays hyperbolically with the length scales shown.

where all the terms of (12) are important and finally the precursor film region (c), where the viscous terms $3H$ and the molecular force term $(\lambda^2/\mathrm{Ca}^2)(H_x/H)$ balance. It is quite questionable that the continuum model holds in the precursor film region (c). We shall merely seek the asymptotic shape of the interface as it approaches the precursor film at the end of the transition region. Introducing the transformation

$$H=3^{2/3}\eta\,, \tag{30a}$$

$$X=3^{1/3}\xi\,, \tag{30b}$$

$$\epsilon=\frac{1}{9}\frac{\lambda^2}{\mathrm{Ca}^2}\,, \tag{30c}$$

(12) becomes

$$\eta^3\eta_{\xi\xi\xi}=\eta+\epsilon\frac{\eta_\xi}{\eta}\,. \tag{31}$$

We are interested in solutions of (31) that satisfy the condition $\eta_{\xi\xi}\to 1$ as $\xi\to-\infty$ in the limit of

$$\epsilon\ll 1\,. \tag{32}$$

In this weak intermolecular force limit, regions (b) and (c) become asymptotically thin and small, such that the film is dominated by region (a), where intermolecular forces play a weak secondary role. The molecular length scale λ dominates in region (c) as $\eta\to 0$, while the length scale $\mathrm{Ca}^{1/3}$ characterizes the lubrication region away from the wall, where viscous forces and surface tension are important. We can see from (12) that such a balance is possible when $\mathrm{Ca}\gg\lambda$, so that the effect of the intermolecular forces away from the solid surface is felt only as a small perturbation. This is a slightly stronger condition than $\mathrm{Ca}^{2/3}\gg\lambda$ for the continuum model to be valid. Again, the velocity of the meniscus is assumed to be large enough such that (32) is satisfied.

In the lubrication region where $\eta\gg 1$, the terms $\eta^3\eta_{\xi\xi\xi}$ and η in (31) balance

$$\eta^3\eta_{\xi\xi\xi}\sim\eta, \quad \text{as } \eta\to+\infty\,. \tag{33}$$

Introducing the transformation

$$\eta_\xi=\Phi(\eta)\,,$$

(33) becomes

$$\Phi(\Phi')^2+\Phi^2\Phi''\sim\frac{1}{\eta^2}\,, \tag{34a}$$

subject to the boundary condition

$$\Phi\Phi'\to 1, \quad \text{as } \eta\to+\infty\,, \tag{34b}$$

where $'=d/d\eta$. The solution to (34a) and (34b) is

$$\Phi\sim-\sqrt{2(\eta-B)}+\frac{2}{3\eta}+\frac{2B}{45\eta^2}\,,$$

$$\text{as } \eta\to+\infty, \quad \xi\to-\infty, \tag{35}$$

where B is an integration constant that can be determined by imposing appropriate boundary conditions to (31) as $\eta\to 0^+$. This is hence a one-parameter family of boundary conditions parametrized by B. Clearly the dominant term of (35) corresponds to a solution with quadratic behavior as $\xi\to-\infty$ and $\eta_\xi<0$. Another solution is also possible with a $+$ sign in front of the leading-order behavior in (35), which, as we will see later, corresponds to a quadratic behavior of the inner region as $\xi\to+\infty$, and therefore has no physical meaning.

Since Tanner's law in (1) seems to be independent of intermolecular forces, it is interesting to see if the solution of (31) can approach the capillary wall smoothly, as required by (14), if ϵ vanishes exactly. In other words, can the film thickness decay smoothly toward the zero in front of the meniscus under viscous and capillary forces only. This is obviously impossible, since if ϵ vanishes, $\eta_{\xi\xi\xi}=\eta^{-2}$, and at least the third derivative will become singular if η vanishes. Actually, even the second derivative can be shown to become singular as η and η_ξ vanish by the following nonlinear coordinate transform due to Voinov,[14] $u(s)=\eta_\xi$, $s=-\ln\eta$, and $Y=uu_s=-\eta\eta_{\xi\xi}$. The transformed equation,

$$\frac{dY}{du}=\frac{1}{Y}-u\,, \tag{36}$$

has the asymptotic behavior

$$Y\sim c+\frac{u}{c}+O(u^2)\,,$$

for u small (η_ξ small), and c is an integration constant. This yields

$$\eta_{\xi\xi}\sim(1/\eta)[-c-\eta_\xi/c+O(\eta_\xi^2)]\,,$$

where the first term in the bracket dominates as $u=\eta_\xi$ vanishes. Hence, if η also vanishes in the same limit, the second derivative must blow up. This then rules out a smooth decay of η toward zero as $\xi\to+\infty$, since this requires all derivatives to vanish. However, the above argument does not rule out a finite-ξ singularity where the zero and first derivatives, vanish, but the second derivative becomes singular. Our numerical integration of (31) with a vanishing ϵ indicates that, with (35) as the initial condi-

This article is copyrighted as indicated in the article. Reuse of AIP content is subject to the terms at: http://scitation.aip.org/termsconditions. Downloaded to IP: 128.118.88.48 On: Fri, 05 Dec 2014 10:14:59

tion for all values of B attempted, the second derivative does blow up as η and η_ξ approach zero at a particular position ξ_0. This corresponds to the formation of a singularity in finite "time" ξ_0. Such singularities violate the lubrication approximation and are unacceptable solutions. Hence it is impossible to have a stationary meniscus whose film decays smoothly in front of it without including intermolecular forces. We will show below that, when intermolecular forces are included, a smooth decay is possible. More interestingly, an asymptotic stationary film profile with the requisite smooth decay in front exists, even for very small values of ϵ. The case of zero ϵ is hence a singular limit since the boundary condition (14) cannot be satisfied from (31) without the molecular force term.

Hence we include the ϵ term and seek the asymptotic behavior of η in (31) as it approaches the precursor film region, where $\eta \to 0^+$ and $\xi \to +\infty$. To satisfy the zero contact condition (14) of the precursor film, the derivatives of η must vanish as ξ approaches $+\infty$. This proper asymptotic behavior can only occur if one can find an asymptotic solution of (31), which receives negligible contribution from the term $\eta^3\eta_{\xi\xi\xi}$. Hence, we remove this term (this assumption can be checked once η is known) and seek a leading-order asymptotic behavior η_0, which satisfies

$$\eta_0 + (\epsilon/\eta_0)\eta_0' \sim 0, \quad \text{as } \xi \to +\infty , \tag{37}$$

where $' = d/d\xi$. The solution to (37) is simply

$$\eta_0 \sim \epsilon/\xi , \tag{38}$$

where the integration constant has been set to zero without loss of generality. Such an asymptotic behavior to (31) has also been derived by Voinov[14] and Hervert and De Gennes.[11] Hence, it is possible to have a hyperbolically decaying smooth film as $\xi \to +\infty$ if intermolecular forces are included. This hyperbolic approach toward the precursor film has been observed in experiments[12] of liquid spreading on high-energy solid surfaces with a large spreading coefficient. In terms of the original variables the region where the molecular forces first become important is characterized by the scalings $z = O(\lambda)$ and $x = O(\lambda/\mathrm{Ca})$ (see Fig. 2). The higher-order corrections to (38) can be successively approximated to yield

$$\eta \sim \frac{\epsilon}{\xi} + \frac{6\epsilon^4}{5\xi^7} + c \exp\left(-\frac{\xi^3}{3\epsilon^{3/2}}\right), \quad \text{as } \xi \to +\infty , \tag{39}$$

which is essentially a one-parameter family of solutions in the asymptotic region where molecular forces first become important. The parameter c can be determined by imposing appropriate boundary conditions as $\xi \to -\infty$. As is obvious from (39), when $\epsilon = 0$ the hyperbolic approach toward the precursor film disappears, as is consistent with our earlier analysis. It is obvious that this hyperbolic decay obeys the boundary condition (14) stipulated, and represents the proper asymptotic behavior of the inner region as $\xi \to +\infty$. It can also be readily shown that this decay corresponds to $|z_x| \sim (3\,\mathrm{Ca})^{1/3}\epsilon/\xi$ and $|z_{xx}| \sim 2\epsilon/\xi^3$ in the original physical variables, such that $|z_x|$ and $|z_{xx}|$ remain small, as required by the lubrication approximation. It also can be easily shown that $\eta^3\eta_{\xi\xi\xi} \sim \epsilon^4\xi^{-7}$ is indeed negligible compared to the other two terms in (31), which are both of order $\epsilon\xi^{-1}$ for (38) or (39), supporting our earlier assumption and indicating that (38) is a possible asymptotic behavior. A solution to (31) with the asymptotic behavior of (38) or (39) is then the appropriate inner solution that must be matched to the outer solution (35).

However, (39) is not the only asymptotic behavior of solutions to (31) when $\eta \ll 1$ and intermolecular forces are included, viz., $\epsilon \neq 0$. Let us assume that there exists a region where the terms $\eta^3\eta_{\xi\xi\xi}$, and $\epsilon\eta^{-1}\eta_\xi$ balance:

$$\eta^3\eta_{\xi\xi\xi} \sim \epsilon\eta^{-1}\eta_\xi , \tag{40}$$

which, after introducing the transformation

$$\eta_\xi = \phi(\eta) , \tag{41}$$

becomes

$$\eta^3(\phi\phi')' \sim \epsilon\eta^{-1} , \tag{42}$$

where $' = d/d\eta$. The solution is simply

$$\phi \sim \pm\sqrt{\tfrac{1}{3}\epsilon\eta^{-2} + c_1\eta + c_2} , \tag{43}$$

where c_1 and c_2 are the constants of integration. When $\eta \to 0^+$, (43) can be approximated by

$$\phi \sim \pm\sqrt{\tfrac{1}{3}\epsilon\eta^{-2}} , \tag{44}$$

where the $-$ sign is pertinent, since it corresponds to $\eta_\xi < 0$. From (44), one simply obtains

$$\eta \sim [c' - 2\xi(\epsilon/3)^{1/2}]^{1/2} , \tag{45}$$

where c' is an integration constant. The above solution is obviously defined for

$$\xi \leqslant \frac{c'}{2(\frac{1}{3}\epsilon)^{1/2}} = \tilde{\xi} , \tag{46}$$

and $\eta_\xi \to -\infty$ as $\xi \to \tilde{\xi}^-$. Like all solutions to (36) with a vanishing η, this solution is also a "finite-time" singularity in ξ, except the singularity appears as early as the first derivative, viz., η_ξ and all the higher-order derivatives exhibit an algebraic pole singularity at $\xi = \tilde{\xi}^-$. We can now verify the assumption $|\eta| \ll |\epsilon\eta^{-1}\eta_\xi|$ used in (40). By using (45) one can easily see that the above condition is satisfied for $|\xi - \tilde{\xi}| \ll (2/16)^{1/3}3^{1/6}\epsilon^{1/2}$, and so (45) is valid only when ξ is very close to $\tilde{\xi}$ which, in general, can be positive or negative. In terms of the original variables, the region described by (45) corresponds to the scalings $z = O(\lambda)$ and $x = O(\lambda)$. Therefore the lateral length scale is much shorter than the one corresponding to (38), while the vertical one is exactly the same (Fig. 2). The presence of a tip region whose behavior is described by (45) has been associated with the existence of a true contact line, which moves with the velocity of the wall.[11,21] However, since this singularity also violates the lubrication approximation and stretches the continuum approximation to the molecular scales at the tip, we shall regard (45) as an unacceptable solution. Hence, the only acceptable solution to the precursor film at infinity is prescribed by (38) or (39), with a smooth delay toward zero. It should be men-

This article is copyrighted as indicated in the article. Reuse of AIP content is subject to the terms at: http://scitation.aip.org/termsconditions. Downloaded to IP: 128.118.88.48 On: Fri, 05 Dec 2014 10:14:59

tioned that one approach to remedy the failure of the continuum approach near the tip is to introduce some cutoff length scale and slope, H_m and Θ_m, for example, immediately above the tip.[14,15] This approach, however, yields contact angles that are dependent on these two unknown quantities. Moreover, it is difficult for us to imagine a physical mechanism by which the motion of the tip, which is highly sensitive to surface roughness, liquid volatility, surface tension, and molecular forces, becomes steady *at* the same speed as the meniscus.

Since the analytical matching of the outer asymptote (35) to (39) is very difficult, in general, because this would involve balance of all the terms in (31), we will numerically integrate (31) for different values of $\epsilon(\ll 1)$. We will use (35) as an initial condition for the integration of (31) toward positive ξ. To leading order, (35) can be written as

$$\eta \sim \tfrac{1}{2}\xi^2 + B, \quad \text{as } \xi \to -\infty , \tag{47}$$

where the constant B is invariant under a translation along the ξ axis and is related to $\tilde{a}$ in (27) by

$$\tilde{a} = 3^{2/3} B . \tag{48}$$

We initiate the integration for different B values to see if (39) can be reached in the positive ξ direction. For a given ϵ, a specific negative value B^* exists, such that for $B < B^*$, the behavior of η can be essentially described by (45) as $\eta \to 0$, while for $B > B^*$, no singularity appears, and the behavior of η as $\xi \to +\infty$ is a quadratic blowup, with $\eta_{\xi\xi}$ approaching a constant whose value depends on B and ϵ [Fig. 3(a)]. The latter behavior corresponds to (35) with a positive sign in front of the leading-order term, and it obviously does not allow proper matching to the precursor film. The correct matching to a decaying film consistent with the asymptotic behavior of (38) or (39) then occurs at B^* exactly. A unique stationary meniscus that satisfies all requisite requirements for a given value of ϵ hence exists at B^*. This meniscus matches into the hyperbolically decaying asymptotic behavior of (38), which yields vanishingly small derivatives of η as $\xi \to +\infty$ and as η approaches zero. However, the other trajectories for $B < B^*$ yield an infinite curvature as η approaches zero, since the singularity (45) is approached. Since the determination of B^* requires the discrimination of trajectories that approach the unacceptable singularity for $B < B^*$, our numerical effort must be able to resolve the horizontal length scales of order $\epsilon^{1/2}$ of these singularities. This places a lower bound on the value of ϵ for the successful construction of the correct meniscus. For relatively high ϵ values ($> 10^{-10}$), the hyperbolic decay at $B = B^*$ can be followed numerically, as shown in Figs. 4(a) and 4(b). These constructed trajectories are favorably compared to the analytical estimate of the asymptotic behavior in (38). For lower ϵ values ($10^{-16} < \epsilon < 10^{-10}$), a unique B^* that demarcates B values that yield a tip with an algebraic singularity and a quadratic blowup of η can still be accurately discerned but the actual hyperbolic decay cannot be followed indefinitely at B^*. This is because η decays as ϵ/ξ as in (38), and our numerical scheme cannot resolve η smaller than 10^{-20}. Nevertheless, the sensitivity of the trajectories near

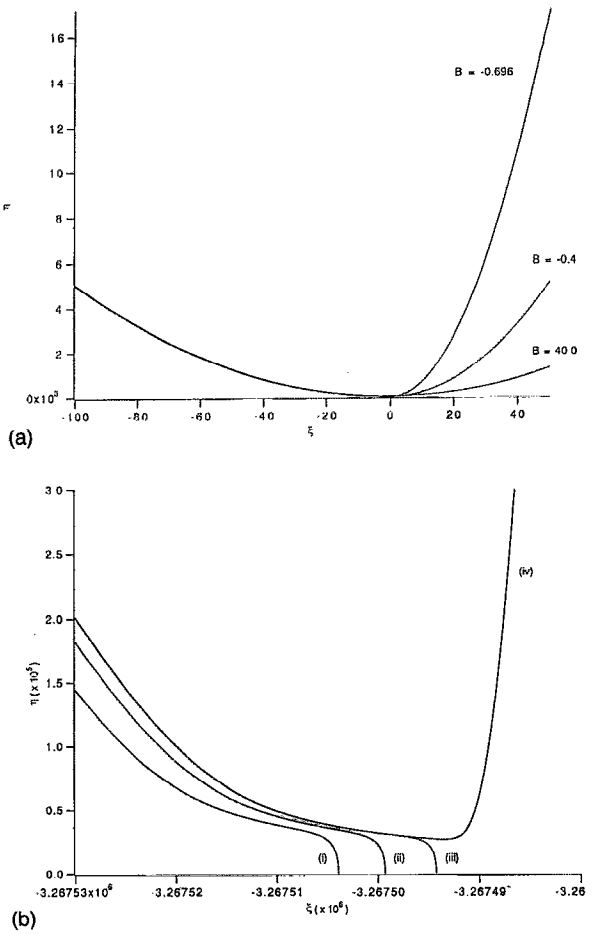

FIG. 3. (a) Typical inner solutions for $\epsilon = 0.5$ and $B > B^*$. Each solution corresponds to the indicated B value used to initiate the integration from $\xi \to -\infty$. The asymptotic solution at large B approaches a unit curvature parabola. These solutions do not allow matching to the precursor film. (b) Inner solutions for B close to B^* for $\epsilon = 10^{-10}$. The values of B are (i) $-5.635\,569$, (ii) $-5.635\,558$, (iii) $-5.635\,552\,8$, and (iv) $-5.635\,552\,7$. The estimated B^* is then between (iii) and (iv), where a hyperbolically decaying film can be matched to a precursor film.

B^* allows us to determine B^* accurately. For $\epsilon < 10^{-16}$, the numerical scheme can no longer resolve the molecular scales at the tip of the singularity (45) and a B^* cannot be found. Fortunately, most practical values of ϵ are larger than 10^{-16}. We have carefully verified the accuracy of the B^* values at small ϵ by changing the precision of our program and by reducing the step size up to 10^{-24} in integrating (31), sufficient to resolve the tip horizontal scale of $\epsilon^{1/2}$, even at $\epsilon = 10^{-16}$. Convergence is achieved in all these tests. Our numerically determined B^* values are shown in Table I and Fig. 5. The dependence of B^* on ϵ is extremely weak. Figure 5(a) shows the variation of B^* as a function of ϵ in a semilog plot. The numerical data in the region $(10^{-16}, 10^{-3})$ can be interpolated with the function

$$|B^*| = 1.8225 + 0.370\,24 \log(1/\epsilon) , \tag{49a}$$

showing that B^* blows up to minus infinity as ϵ approaches zero. However, this ϵ dependence is very weak and ϵ must be extremely small (smaller than most practical values and below our numerical resolution) for $|B^*|$ to be very large. In all practical applications, ϵ takes on values

This article is copyrighted as indicated in the article. Reuse of AIP content is subject to the terms at: http://scitation.aip.org/termsconditions. Downloaded to IP: 128.118.88.48 On: Fri, 05 Dec 2014 10:14:59

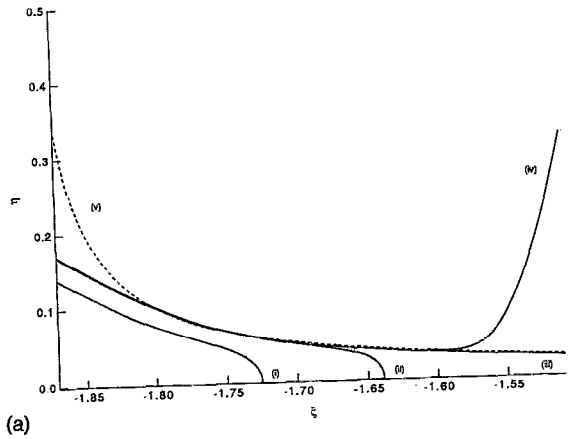

(a)

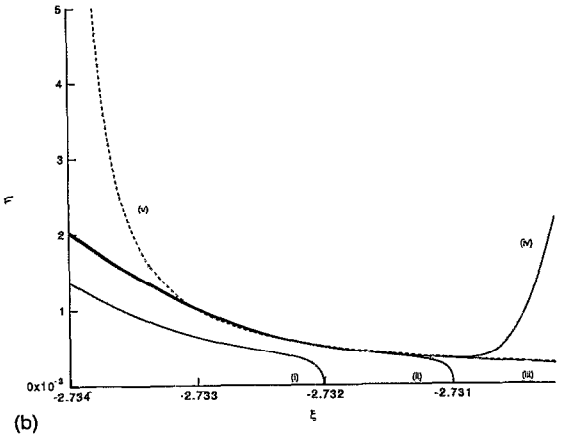

(b)

FIG. 4. (a) Inner solutions for B close to B^* for $\epsilon=10^{-2}$. The values of B are (i) -2.13, (ii) -2.089, (iii) $-2.087\,250\,846\,310\,4$, and (iv) $-2.087\,245$, (v) is the hyperbolically decaying precursor film $\epsilon/(\xi-\xi_0)$ at large ξ with the apparent origin $\xi_0=-1.9$. The estimated B^* is between (iii) and (iv). (b) Inner solutions for B close to B^* for $\epsilon=10^{-6}$. The values of B are (i) -4.107, (ii) -4.1055, (iii) $-4.105\,443\,540\,490\,8$, and (iv) $-4.105\,44$, (v) is the hyperbolically decaying precursor film $\epsilon/(\xi-\xi_0)$ with $\xi_0=-2.734$. The estimated B^* is between (iii) and (iv).

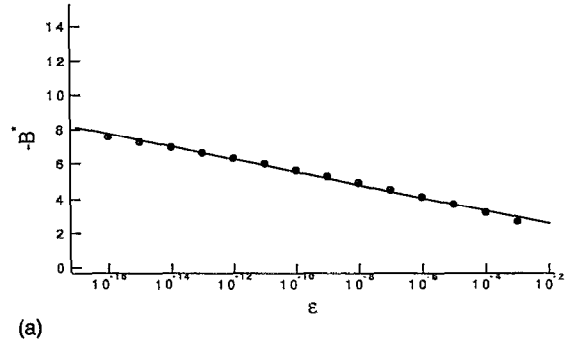

(a)

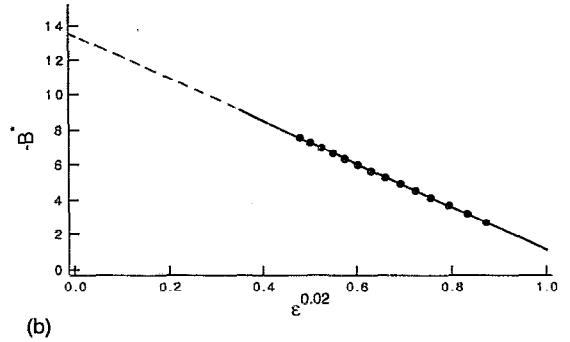

(b)

FIG. 5. (a) The dependence of $B^*(\epsilon)$ on ϵ and correlation (49a). As ϵ approaches zero $|B^*|$ blows up. (b) The dependence of $B^*(\epsilon)$ on ϵ and correlation (49b). An apparent constant asymptote is reached as ϵ approaches zero.

TABLE I. Computed B^* values.

ϵ	$-B^*$
$1.000\,00\times10^{-1}$	1.356
$1.000\,00\times10^{-2}$	2.088
$1.000\,00\times10^{-3}$	2.683
$1.000\,00\times10^{-4}$	3.201
$1.000\,00\times10^{-5}$	3.671
$1.000\,00\times10^{-6}$	4.106
$1.000\,00\times10^{-7}$	4.515
$1.000\,00\times10^{-8}$	4.905
$1.000\,00\times10^{-9}$	5.277
$1.000\,00\times10^{-10}$	5.636
$1.000\,00\times10^{-11}$	5.983
$1.000\,00\times10^{-12}$	6.319
$1.000\,00\times10^{-13}$	6.645
$1.000\,00\times10^{-14}$	6.964
$1.000\,00\times10^{-15}$	7.274
$1.000\,00\times10^{-16}$	7.578

in the interval $[10^{-16}, 10^{-1}]$ of Table I. Furthermore, we can express the data of Table I in a different way. We can assume that $|B^*|$ is a function of ϵ^{α} as $\epsilon\to0$. The value $\alpha=0.02$ makes this function a straight line, as is shown in Fig. 5(b),

$$|B^*|=13.444-12.340\epsilon^{0.02}, \tag{49b}$$

so that B^* approaches an *apparent* limit with the value -13.444 when the straight line (49b) is extrapolated toward $\epsilon=0$. This limit is not a real one, however, as we have shown that (31) with $\epsilon=0$ exactly does not yield the proper decay at $\xi=\infty$, viz., $\epsilon=0$ is a singular limit. Nevertheless, this apparent limit is a tight upper bound of B^* in the limit $\mathrm{Ca}\gg\lambda$, viz., $\epsilon\ll1$ or thick films. The weak dependence of B^* on ϵ as ϵ approaches zero is the basic reason why Tanner's law is practically independent of intermolecular forces, and hence applies to all wetting fluids. The shape of the inner solution at $\epsilon=10^{-16}$ is shown in Fig. 6. It includes the hyperbolic approach toward the precursor film at small ϵ value and the capillary/viscous region in the lubricating film region.

V. THE APPARENT DYNAMIC CONTACT ANGLE

We define the apparent contact angle as

$$\cos\Theta=\frac{1}{R_c}, \tag{50}$$

This article is copyrighted as indicated in the article. Reuse of AIP content is subject to the terms at: http://scitation.aip.org/termsconditions. Downloaded to IP: 128.118.88.48 On: Fri, 05 Dec 2014 10:14:59

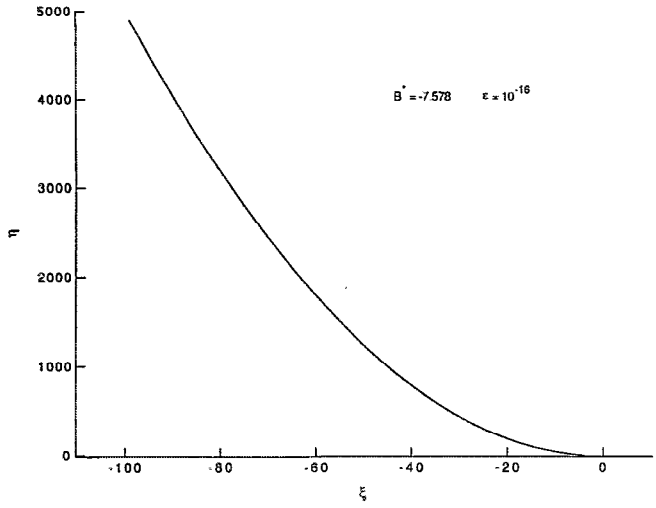

FIG. 6. The shape of the inner solution for $\epsilon=10^{-16}$.

where R_c, shown in Fig. 1, is the radius of axial curvature at the point where the outer region makes contact with the wall. From the numerical construction of the inner region, we find that $B^*<0$, and so the constant term $\tilde{a}$ in (27) is also always negative. When extrapolated backward, the parabola defined by (27) intersects the wall, since $H(X=0)=\tilde{a}<0$. Equation (50) is identical to the measurement technique used by Hoffman,[7] where R_c is the actual radius of the circle that the liquid–air interface forms. Therefore, what is really measured experimentally is not the asymptotic slope of the inner region (Friz's theory) away from the wall, but rather the angle that the outer region forms with the wall after the matching, since the inner region is practically invisible (~ 0.001 cm for $R_0\sim 0.1$ cm and $\mathrm{Ca}\sim 10^{-3}$).

With $r=-h$, where h refers to the lower half of the liquid–air interface in Fig. 1, and using only the axial curvature, we have

$$\frac{1}{R_c}=\left(\frac{h_{xx}}{(1+h_x^2)^{3/2}}\right)_{x=1}, \tag{51}$$

where the curvature is evaluated at $x=1$, since $R_c=\mathrm{OA}=\mathrm{O\Gamma}$ (Fig. 1). With the substitution $h=h_0+\mathrm{Ca}^{2/3}h_2$, where h_0 and h_2 are known from the matching, one obtains

$$\cos\Theta=1+\tilde{a}\,\mathrm{Ca}^{2/3}+O(\mathrm{Ca}^{4/3}), \tag{52}$$

which can also be written as

$$\tan\Theta=-\sqrt{-2\tilde{a}}\,\mathrm{Ca}^{1/3}, \tag{53}$$

where terms $O(\mathrm{Ca}^{2/3})$ have been neglected. Alternatively, (53) can be derived by evaluating the slope of the inner region (27) at the point $X_0=-(-2\tilde{a})^{1/2}$, where $H=0$. This is the proper location of the inner solution for the evaluation of the apparent dynamic contact angle. We can also derive (53) by determining the exact location of point A in Fig. 1 where the outer region (dotted line) intersects the wall. If the coordinate of point A is denoted with x_A, then x_A is a solution of the equation $r(x_A)=1$, or by using (15a), (18), and (28) x_A can be found from

$$1-(1-x_A)^2-\tilde{a}\,x_A\,\mathrm{Ca}^{2/3}=[1-(1-x_A)^2]^{1/2}, \tag{54}$$

which with $x_A=1-x_0\,\mathrm{Ca}^{1/3}+O(\mathrm{Ca}^{2/3})$ gives $x_0=\sqrt{-2\tilde{a}}$. We can then estimate the angle Θ that the tangential line at point A forms with the wall from $|\tan\Theta|=|dr(x_A)/dx|$, which leads to $|\tan\Theta|=x_0\,\mathrm{Ca}^{1/3}$, which is exactly (53). We can now assume that the perpendicular to the tangential line at point A of Fig. 1 does not pass through O, so that the center of curvature at A is some other point O′. We have already shown that $x_A=1-|\tan\Theta|$. Then $|\tan\angle\mathrm{AOB}|=\mathrm{AB/OB}=\mathrm{AB}$ and $x_A=1-(\mathrm{AB})$, so that $\angle\mathrm{AOB}=\Theta$. If now the projection of O′ on the wall is B′, then O′B′ should be parallel to OB, and since the points B and B′ are different, O′A should be parallel to OA, or, in other words, the points O and O′ should be identical up to $O(\mathrm{Ca}^{1/3})$. For higher capillary numbers, the two centers of curvature are expected to be different, with the distance O′O being analogous to $O(\mathrm{Ca}^{2/3})$. It should also be pointed out that $2\cos\Theta$ is essentially the pressure drop across the interface,

$$\Delta P=2+2\tilde{a}\,\mathrm{Ca}^{2/3}. \tag{55}$$

Substituting (49a) into (48) and (53), we obtain

$$|\tan\Theta|=[7.582+1.540\log(1/\epsilon)]^{1/2}\,\mathrm{Ca}^{1/3}, \tag{56a}$$

while substituting (49b) into (48) and (53), we obtain

$$|\tan\Theta|=7.48\,\mathrm{Ca}^{1/3}-3.28\lambda^{0.04}\,\mathrm{Ca}^{0.293}, \tag{56b}$$

where

$$\lambda=R_m/R_0$$

is the dimensionless molecular length scale. The value of R_m for most liquids is at the Ångström level, which is far smaller than the capillary radius. Consequently, in the limit of $\mathrm{Ca}\gg\lambda$, which is consistent with $\epsilon\ll 1$ of (32), (56b) yields

$$|\tan\Theta|=7.48\,\mathrm{Ca}^{1/3}. \tag{57}$$

Away from this limit, (56b) suggests that the contact angle is a weak function of λ with convergence to (57) from below for $\epsilon\ll 1$. As we have shown, this corresponds to an *apparent* limit and not a real one. A typical value for λ for a fluid with $\sigma\sim 20$ dyn/cm and a capillary radius R_0 of 1 mm is 5.0×10^{-8}, corresponding to $|A|\sim 10^{-14}$ ergs. This value of the Hamaker constant is an approximate upper bound for wetting fluids. A dashed line corresponding to (56a) with $\lambda=5.0\times 10^{-8}$ is shown in Fig. 7. It is very close to the asymptotic behavior of (57), as expected, and the relative correction to the asymptotic value decreases with increasing Ca and increasing thickness of the lubricating film. A slight correction to the $\mathrm{Ca}^{1/3}$ behavior occurs at low Ca values. Since most wetting fluids have Hamaker constants that can be orders of magnitude lower than this value, one hence expects (57) to be a good representation of most fluids. Hence, we have derived the constant in front of Tanner's law (1) for the apparent contact angle of a meniscus in a capillary.

This article is copyrighted as indicated in the article. Reuse of AIP content is subject to the terms at: http://scitation.aip.org/termsconditions. Downloaded to IP: 128.118.88.48 On: Fri, 05 Dec 2014 10:14:59

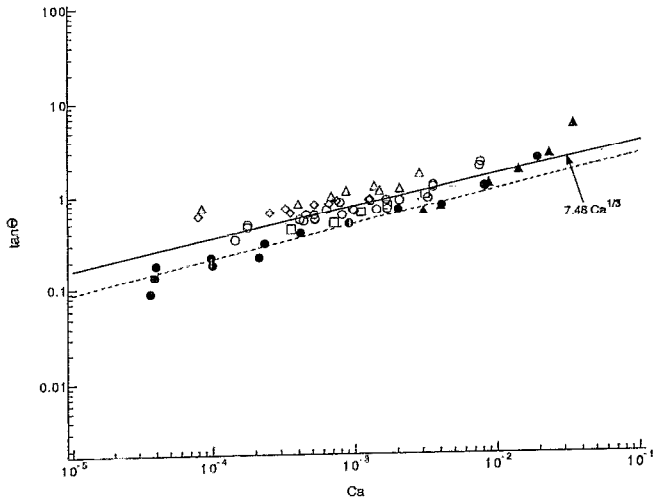

FIG. 7. Renormalization of contact angle data of Hoffman[7] (solid markers—perfect wetting) and Rose and Heinz[9] (open markers—prewetted capillary) by the correlation $\tan\Theta=7.48\,\mathrm{Ca}^{1/3}$, for different liquids and different capillary radii: (●) G. E. silicone SF-96, $2R_0=0.196$ cm; (▲) Brookfield silicone, $2R_0=0.196$ cm; (○) Nujol, $2R_0=0.066$ cm; (□) Nujol, $2R_0=0.110$ cm; (△) oleic acid, $2R_0=0.100$ cm; (◇) oleic acid, $2R_0=0.066$ cm. The dashed line corresponds to (56a), which includes intermolecular forces for G.E. silicone SF-96 with $\lambda=5.0\times10^{-8}$.

The proper normalization of all apparent contact angle data for a meniscus in a capillary (Hoffman[7] and Rose and Heinz[9]) by (57) is shown in Fig. 7, where (56a) is also shown for comparison. The solid symbols correspond to wetting fluids, which seem to feel the small effects of intermolecular forces as they diverge from (57) in the manner described by (56b), while the others are for partially nonwetting fluids. Even the predicted slight change to the $\mathrm{Ca}^{1/3}$ dependence at low Ca is shown by the wetting fluids. For the latter, the capillary is prewetted in the experiment, such that the apparent dynamic contact angle approaches zero with Ca. This is carried out by moving the meniscus back and forth before a steady forward motion is created. The prewetting introduces a vanishingly thin film in front of the meniscus if the experiment is carried out before film rupture sets in. Steady motion of a meniscus that approaches a vanishingly thin film in front is exactly the problem we analyzed, and, not surprisingly, even these nonwetting fluids, whose true static contact angles do not vanish, are well described by (57) or (56). The agreement extends to $\mathrm{Ca}\sim10^{-2}$ with $\Theta\sim60°$, where the long-wave lubrication approximation begins to break down and the meniscus speed is probably of the same order as the wetting speed of the precursor film. The curvature of the meniscus inverts rapidly at this extreme as Θ increases from 60° to 90° and Ca increases from 2.0×10^{-2} to about 3.0×10^{-2}. Beyond this Ca value, Θ is in excess of 90° and the lubricating liquid film in front of the meniscus in Fig. 1 is replaced by a gas film behind the inverted meniscus.

VI. SUMMARY AND CONCLUSION

We have carried out the proper matched asymptotic analysis that matches the static outer region to the precursor film through the lubricating film at the inner region. The inner region is dominated by viscous and capillary forces. At the front of this region, however, intermolecular forces and a vanishingly small film spread by fast wetting stipulate a hyperbolic decay of the film thickness toward zero. We obtain a unique universal correlation for the apparent contact angle in (57) in the limit of thick films that agrees with the observed values. At lower Ca the apparent dynamic contact angle has a weak dependence on the intermolecular interactions. If the film can be experimentally resolved, its shape should also be in quantitative agreement with the curve in Fig. 6. It would be difficult to numerically resolve the widely varying length scales of the present problem as shown in Figs. 1 and 2. The precursor film would definitely require molecular dynamics simulation. However, the problem is extremely amenable to matched asymptotic analysis precisely because of the three length scales: the capillary radius, the $\mathrm{Ca}^{2/3}$ film thickness, and the λ molecular scale. The important limit of a vanishingly thin film spread by fast wetting ($S\to\infty$) with negligible intermolecular forces ($\epsilon\to0^+$) also removes the necessity of resolving the molecular dynamics at the precursor film. The hyperbolic decay pertains to the necessary behavior of the lubricating film as it approaches the molecular scales of the precursor film, where the continuum model becomes invalid. Explicit knowledge of the detailed molecular dynamics in the precursor film is not required for the analysis, and this also accounts for the universal character of (57) for a wide range of fluids, as shown in Fig. 7. We can easily link (57) or (56) to a popular slip model to yield a slip boundary condition. If the traction exerted by the fluid on the solid surface is expressed as $\tau=\beta(v-U)$, where β is the slip coefficient and v is the fluid velocity on the wall, then the solution of the Stokes approximation, with the assumption that the fluid makes a contact with the wall at an angle θ (the actual dynamic contact angle of the contact line), provides a relation $\Theta=\Theta(\theta, \mathrm{Ca}, R_0, L_s)$, where L_s is the slip length scale defined as μ/β. Then by setting θ equal to zero for a case of a wetting fluid, and by substituting Θ from (57) or (56), we can obtain the slip coefficient β as a function of Ca. However, one must recall that the slip model is needed to resolve the interface shape and the flow field in the outer region. Both are already offered by our matched asymptotic analysis, and the need for a relation $\beta=\beta(\mathrm{Ca})$ seems limited. Finally, it is interesting to address the problem of a receding meniscus with a negative U in Fig. 1. The difference in the positive and negative U behavior may shed light on apparent contact angle hysteresis at low Ca. Our preliminary analysis yields a positive B^* for the receding problem, indicating the apparent contact angle is zero up to $O(\mathrm{Ca}^{1/3})$ and nonzero contact angles exist at $O(\mathrm{Ca}^{2/3})$. However, while this analysis shows that the advancing and receding menisci behave differently, higher-order analysis of the later requires consideration of slope correction to the intermolecular force.[20] The possible hysteresis behavior hence involves a more detailed study.

This article is copyrighted as indicated in the article. Reuse of AIP content is subject to the terms at: http://scitation.aip.org/termsconditions. Downloaded to IP: 128.118.88.48 On: Fri, 05 Dec 2014 10:14:59

ACKNOWLEDGMENT

This work is supported by the U. S. Department of Energy through Grant No. DE-FG02-92ER14269.

[1]E. B. Dussan V., "On the spreading of liquids on solid surfaces: Static and dynamic contact lines," Annu. Rev. Fluid Mech. **11**, 371 (1979).
[2]H. K. Moffatt, "Viscous and resistive eddies near a sharp corner," J. Fluid Mech. **18**, 1 (1963).
[3]C. Huh and L. E. Scriven, "Hydrodynamic model of steady movement of a solid/liquid/fluid contact line," J. Colloid Interface Sci. **35**, 85 (1971).
[4]L. M. Hocking, "A moving fluid interface. Part 2. The removal of the force singularity by a slip flow," J. Fluid Mech. **79**, 209 (1977).
[5]C. G. Ngan and E. B. Dussan, V, "On the dynamics of liquid spreading on solid surfaces," J. Fluid Mech. **209**, 191 (1989).
[6]E. B. Dussan, V, "The moving contact line: The slip boundary condition," J. Fluid Mech. **77**, 665 (1976).
[7]R. L. Hoffman, "A study of the advancing interface I. Interface shape in liquid–gas systems," J. Colloid Interface Sci. **50**, 228 (1975).
[8]L. Tanner, "The spreading of silicone oil drops on horizontal surfaces," J. Phys. D **12**, 1473 (1979).
[9]W. Rose and R. W. Heinz, "Moving interfaces and contact angle rate dependency," J. Colloid Sci. **17**, 39 (1962).
[10]F. P. Bretherton, "The motion of long bubbles in tubes," J. Fluid Mech. **10**, 166 (1961).
[11]H. Hervert and P. G. De Gennes, "Dynamique du mouillage: Films précurseurs sur solide ⟨⟨sec⟩⟩," Comptes Rendus, Sér. II **299**, 499 (1984).
[12]D. Ausserré, A. M. Picard, and L. Léger, "Existence and role of the precursor film in the spreading of polymer liquids," Phys. Rev. Lett. **57**, 2671 (1986).
[13]J. A. Nieminen, D. B. Abraham, M. Karttunen, and K. Kaski, "Molecular dynamics of a microscopic droplet on solid surface," Phys. Rev. Lett. **69**, 124 (1992).
[14]O. V. Voinov, "Inclination angles of the boundary in moving liquid layers," Zh. Prikl. Mekh. Tekh. Fiz. **2**, 92 (1977).
[15]P. G. De Gennes, "Dynamique d'étalement d'une goutte," Comptes Rendus Sér. II **298**, 111 (1984).
[16]G. Friz, "Über den dynamischen randwinkel im fall der vollständigen benetzung," Z. Angew. Phys. **19**, 374 (1965).
[17]C.-W. Park and G. M. Homsy, "Two-phase displacement in Hele Shaw cells: Theory," J. Fluid Mech. **139**, 291 (1984).
[18]S. Davis, "Rupture of thin liquid films," in *Waves on Fluid Interfaces*, edited by R. E. Meyer (Academic, New York, 1982), p. 291.
[19]C. A. Miller and P. Neogi, *Interfacial Phenomena* (Dekker, New York, 1985).
[20]L. M. Hocking, "The influence of intermolecular forces on thin fluid layers," Phys. Fluids A **5**, 793 (1993).
[21]J. F. Joanny and P. G. De Gennes, "Structure statique des films de mouillage et des lignes de contact," Comptes Rendus Sér. II **299**, 279 (1984).

This article is copyrighted as indicated in the article. Reuse of AIP content is subject to the terms at: http://scitation.aip.org/termsconditions. Downloaded to IP: 128.118.88.48 On: Fri, 05 Dec 2014 10:14:59